AFRL-RH-FS-TR-2023-0021

Suprathreshold Retinal Lesions Induced by a Continuous-Wave 1070 nm Laser

Francesco J. Echeverria
Semih S. Kumru
Benjamin A. Rockwell
Morgan S. Schmidt
711th Human Performance Wing
Human Effectiveness Directorate
Bioeffects Division
Optical Radiation Bioeffects Branch

Brian J. Lund
Amanda M. Peterson
Harvey M. Hodnett
Gary D. Noojin
SAIC

Amanda J. Tijerina
CMI

31 August 2023
Interim Report for November 2020 to December 2020

Air Force Research Laboratory
711th Human Performance Wing
Human Effectiveness Directorate
Bioeffects Division
Optical Radiation Bioeffects Branch
JBSA Fort Sam Houston, Texas 78234

NOTICE AND SIGNATURE PAGE

Using Government drawings, specifications, or other data included in this document for any purpose other than Government procurement does not in any way obligate the U.S. Government. The fact that the Government formulated or supplied the drawings, specifications, or other data does not license the holder or any other person or corporations; or convey any rights or permission to manufacture, use, or sell any patented invention that may relate to them.

This report was cleared for public release by the AFRL Public Affairs Office and is available to the general public, including foreign nationals. Copies may be obtained from the Defense Technical Information Center (DTIC) (http://www.dtic.mil).

"Suprathreshold Retinal Lesions Induced by a Continuous-Wave 1070 nm Laser"

(AFRL-RH-FS-TR- 2023- 0021) has been reviewed and is approved for publication in accordance with assigned distribution statement.

FERRIS.LYNDSEY.MARIE.1381070391 Digitally signed by FERRIS.LYNDSEY.MARIE.1381070391 Date: 2023.09.27 08:50:45 -05'00'

LYNDSEY M. FERRIS, LtCol, USAF, BSC
Chief, Optical Radiation Bioeffects Branch

MILLER.STEPHANIE.A.1230536283 Digitally signed by MILLER.STEPHANIE.A.1230536283 Date: 2023.12.07 09:25:25 -06'00'

STEPHANIE A. MILLER, DR-IV, DAF
Chief, Bioeffects Division
Airman Systems Directorate
711th Human Performance Wing
Air Force Research Laboratory

This report is published in the interest of scientific and technical information exchange, and its publication does not constitute an official position of the U.S. Government.

REPORT DOCUMENTATION PAGE

Form Approved
OMB No. 0704-0188

1. REPORT DATE *(DD-MM-YYYY)*	**2. REPORT TYPE**	**3. DATES COVERED** *(From - To)*
11-08-2022	Interim Technical Report	November 2020 to December 2020

4. TITLE AND SUBTITLE
Suprathreshold Retinal Lesions Induced by a Continuous-Wave 1070 nm Laser

5a. CONTRACT NUMBER
FA8650-19-C-6024

5b. GRANT NUMBER

5c. PROGRAM ELEMENT NUMBER

6. AUTHOR(S)
Francesco J. Echeverria, Semi S. Kumru, Benjamin A. Rockwell, Morgan S. Schmidt, Brian J. Lund, Harvey M. Hodnett, Amanda M. Peterson, Gary D. Noojin, Amanda S. Tijerina

5d. PROJECT NUMBER

5e. TASK NUMBER

5f. WORK UNIT NUMBER
H14B

7. PERFORMING ORGANIZATION NAME(S) AND ADDRESS(ES)
Air Force Research Laboratory
711th Human Performance Wing
Human Effectiveness Directorate
Bioeffects Division
Optical Radiation Branch
JBSA, Fort Sam Houston, Texas 78234

SAIC
4141 Petroleum Rd
Fort Sam Houston, Texas 78234

8. PERFORMING ORGANIZATION REPORT

9. SPONSORING / MONITORING AGENCY NAME(S) AND ADDRESS(ES)
711th Human Performance Wing
Human Effectiveness Directorate
Bioeffects Division
Optical Radiation Branch
JBSA, Fort Sam Houston, Texas 78234

10. SPONSOR/MONITOR'S ACRONYM(S)
711 HPW/RHDO

11. SPONSOR/MONITOR'S REPORT NUMBER(S)
AFRL-RH-FS-TR-2023-0021

12. DISTRIBUTION / AVAILABILITY STATEMENT
Distribution Statement A. Distribution for public release; distribution in unlimited. CLEARED: PA Case# AFRL-2023-1158. The views expressed are those of the author and do not necessarily reflect the official policy or position of the Department of the Air Force, the Department of Defense, or the U.S government

13. SUPPLEMENTARY NOTES

14. ABSTRACT
Threshold and suprathreshold effects of retinal exposure to a 1070 nm wavelength continuous-wave laser were investigated using a Yucatan mini-pig model. The exposure duration was 100 ms. The ED_{50} for inducing a retinal injury was 29.9 mJ total intraocular energy (TIE). Suprathreshold exposures up to 1 J TIE did not produce hemorrhagic lesions. However, the lesion size did correspond to the laser dose.

15. SUBJECT TERMS

16. SECURITY CLASSIFICATION OF:			**17. LIMITATION OF ABSTRACT**	**18. NUMBER OF PAGES**	**19a. NAME OF RESPONSIBLE PERSON**
Unclassified					Dr. Emily Boice
a. REPORT	**b. ABSTRACT**	**c. THIS PAGE**	U	27	**19b. TELEPHONE NUMBER** *(include area code)*
U	U	U			

Animal Care and Use

The animals involved in this study were procured, maintained, and used according to an Institutional Animal Care and Use Committee (IACUC)-approved Animal Use Protocol and established animal welfare standards, compliant with: DoD Instruction 3216.01 (DoD, 2019); U.S. Department of Agriculture Animal Welfare Regulations (USDA, 2022); The Guide for the Care and Use of Laboratory Animals, 8th Edition, National Research Council (2011); and DHA-MSR 6025.02 (Defense Health Agency, 2022). The Air Force Research Laboratory at Joint Base San Antonio (JBSA) Fort Sam Houston, Texas has been accredited by AAALAC International since 1967.

TABLE OF CONTENTS

List of Figures

Page

Imagery in this document are property of the U.S. Air Force.

List of Tables

Imagery in this document are property of the U. S. Air Force.

1 INTRODUCTION

This is the second report on a study of the effects of suprathreshold retinal laser exposure. In the first report [1], Yucatan mini-pig retinas were exposed to a q-switched Nd:YAG laser (7 ns pulses, 1064 nm wavelength). The previous study determined a minimal visible lesion (MVL) for nanosecond pulse 1064 nm laser exposures. These generally appear as small areas of hypopigmentation. As pulse energy increases, we begin to observe sub-retinal, or contained hemorrhagic lesions (CHL). In a CHL, blood vessels of the choroid rupture and blood pools under the retina creating edema but does not perforate the retina. At even higher pulse energies, the retina ruptures and blood leaks in to the vitreous – a vitreal hemorrhage lesion (VHL). The doses for these effects were sufficiently separated to be able to determine separate ED_{50} values for inducing an MVL, CHL or VHL in the pig retina.

In this report, we consider the suprathreshold effects of exposure to a continuous-wave (CW) near-infrared solid-state laser (1070 nm, 100 ms exposures). In this case, we did not observe clearly resolved hemorrhagic effects (CHL or VHL). We hypothesize the long CW exposure generates enough heat to cauterize any damaged capillaries or other blood vessels, preventing the leakage and accumulation of blood. Rather, the damage is of the nature of a thermal denaturation of the tissue, with the area of retina affected increasing in size with an increase in dose.

This study also represents a continuation of the development and validation of the Yucatan mini-pig eye as a replacement for the use of non-human primates (NHPs) to study retinal effects. As such, the MVL ED_{50} measured here in the pig eye is compared to data from similar exposures in NHP eyes. The reader is referred to Schmidt, et al. [1] for a discussion of the rationale for using a Yucatan mini-pig model.

Finally, this study provides data for the validation of physics-based models of scalable laser effects in development by the Optical Radiation Bioeffects Branch.

2 METHODS

The 1070-nm laser retinal exposure damage threshold study was conducted at JBSA Fort Sam Houston, TX. The parts of this section include animal preparation, experimental setup, and experimental procedures.

2.1 Animal Model

Female Yucatan mini-pigs (*Sus scrofa domestica*), ranging in age from 3 to 6 months, were used for this study. The animals involved in this study were procured, maintained, and used according to an Institutional Animal Care and Use Committee (IACUC)-approved Animal Use Protocol and established animal welfare standards, compliant with: DoD Instruction 3216.01 [2]; US Department of Agriculture Animal Welfare Regulations [3]; The Guide for the Care and Use of Laboratory Animals, 8th Edition, National Research Council [4]; and AFMAN 40-401(1) [5]. The Air Force Research Laboratory at Joint Base San Antonio (JBSA) Fort Sam Houston, Texas has been accredited by AAALAC, International since 1967.

For all procedures, subjects were first sedated with 4-6 mg/kg Telazol® (Tilzolan, Dechra Vet Products, #17033001005, 100mg/mL when reconstituted in 5mL sterile H_2O (Pfizer Inc, #00409-4887-99)) using a 23-gauge winged infusion set (Jorgenson Labs Inc., #JO454C, blue) with a 3 mL syringe (Monoject, 8881250305). Anesthesia was then induced and maintained using Isofluorange gas anesthetic (2% Isofluroane, 1% Oxygen). Anesthesia was maintained throughout all procedures on a given day. For example, on a day of retinal exposures, the subject was maintained under anesthesia continuously through the baseline fundus imaging, retinal exposures, and 1-hour post-exposure examination and imaging.

Vital signs and temperature of the subject were continuously monitored during procedures. A Hot Dog Multifunctional Controller System (WC53) warmed blankets and the subjects.

The subject's eyes were dilated and cycloplegia induced for imaging and laser exposure by first applying two drops of Proparacaine HCl 0.5% Ophthalmic Solution, USP (Bausch Health US, NDC24208-730-06). Then two drops each of Tropicamide Ophthalmic Solution 1%, USP (Sandoz, NDC61314-355-02) and Phenylephrine HCl Opthalmic Solution 2.5%, USP (Paragon, NDC42702-102-15) were applied. A generous amount of GenTeal Gel, severe (Alcon Laboratories Inc., NDC0078-0429-47) was administered to both eyes. Next, both eyes were closed and secured with gauze (Dermacea, #441217) and surgical tape (3M Transpore, #1527-1).

A 15 mm Barraquer wire lid speculum (RICA Surgical Products Inc., #1-1835) held the eye open for imaging and exposure. During procedures, the eye was periodically irrigated with normal saline (sodium chloride 0.9%, Hospira NDC0409-7983-03) to lubricate the eye and maintain clarity of the cornea. When moving the subject between the imaging and exposure laboratories, or during the waiting period between the last exposure and the beginning of the 1-hour post-exposure examination, the speculum was removed, GenTeal Gel was applied to the cornea, and the eyelid secured as described above.

To perform the retinal laser exposures, the subject was placed on a stage with its chin mounted on a higher plane to allow for beam access to the eye. The eye to be exposed was uncovered, and peribulbar injections were administered to reduce extraocular muscular movement that occur, even while under anesthesia. A 3 mL syringe with 25-gauge needle containing 1.5 mL Lidocaine HCl 2% (Phoenix, NDC57319-533-06) and was administered as follows: 0.75 mL on top of eye and 0.75 mL below eye. If repeated eye movement occurred due to prolonged experiments, proparacaine drops were re-administered and after 1 minute, the peribulbar injections were repeated as follows: 0.25 mL on top and 0.25 mL below eye so as not to exceed the maximum dose 2 mL of lidocaine for a single eye per day.

Procedures were conducted on only one of a subject's eyes at a time. The first eye of each subject was used to collect data to measure the MVL ED_{50}. These procedures encompassed two days. On day 1, baseline imaging, retinal laser exposures, and the 1-hour post-exposure imaging and evaluation occurred. On day 2, the 24-hour post-exposure imaging and evaluation was performed.

The second eye of each subject received suprathreshold exposures. These procedures took place on one day. Following the 1-hour post-exposure evaluation and imaging, and while still under anesthesia, the subject was euthanized. The eyes were exenterated and preserved for future histology.

2.2 Experimental Setup

The following section includes details for the laser set-up for exposures, beam characterization, the estimation of retinal spot size, the general laser exposure procedures, and the evaluation of exposure sites.

2.2.1 Laser Setup for 1070 nm Retinal Laser Experiments

The experimental setup for exposing the porcine retinas is illustrated in **Figure 1**. A Spectra Physics VGEN-C-20 laser delivered single 1070 nm wavelength, 100 ms duration pulses to the subject's retina. A Galilean telescope, consisting of lenses L1 and L2 in Figure 1**,** collimated the 1070 nm laser and reduced the beam diameter from 6 mm to 2.5 mm. A low-power co-aligned visible wavelength (635 nm) beam from a continuous wave (CW) helium neon (HeNe) laser aided in aligning the delivery optics, and in selecting sites for retinal exposures. A neutral density filter (Filter in Figure 1) attenuated the HeNe beam to the minimum level that allowed beam alignment and selection of exposure sites.

The entire laser apparatus mounted to a series of linear and rotational stages affixed to the top of the fundus camera. BS2 in Figure 1 aligned the co-aligned laser beams with the optical axis of the fundus camera. Maneuvering the fundus camera across the horizontal and vertical planes selected different locations on the retina for laser exposure. A manually operated shutter installed in the 1070 nm laser path was an additional safety control.

Beam splitter BS1 directed a portion of the pulse energy into a Coherent PM3, used as a reference detector (Ref), to calculate the energy dose delivered to the eye. Placing a Coherent PM10 sensor in the target (eye) position calibrated the reference detector prior to placing an animal subject in the exposure system. Collecting data covering the range of pulse energies used during the exposure session measured the ratio of reference energy to target energy. A series of neutral density filters (NDF) achieved the broad range of pulse energies delivered to the target.

Custom LabView (National Instruments) software controlled the output energy of the VGEN, allowing for finer pulse energy increments, as well as controlling laser firing and recording the reference energy and time of the exposure. This software also recorded live videos of the laser exposures, aiding the future identification of any contained (CHL) or vitreal (VHL) hemorrhages, and providing a reference to help identify exposure sites for non-hemorrhagic exposures.

APPENDIX A contains a list of the detectors and meters used to record the dose for each exposures and calibrate the reference detector.

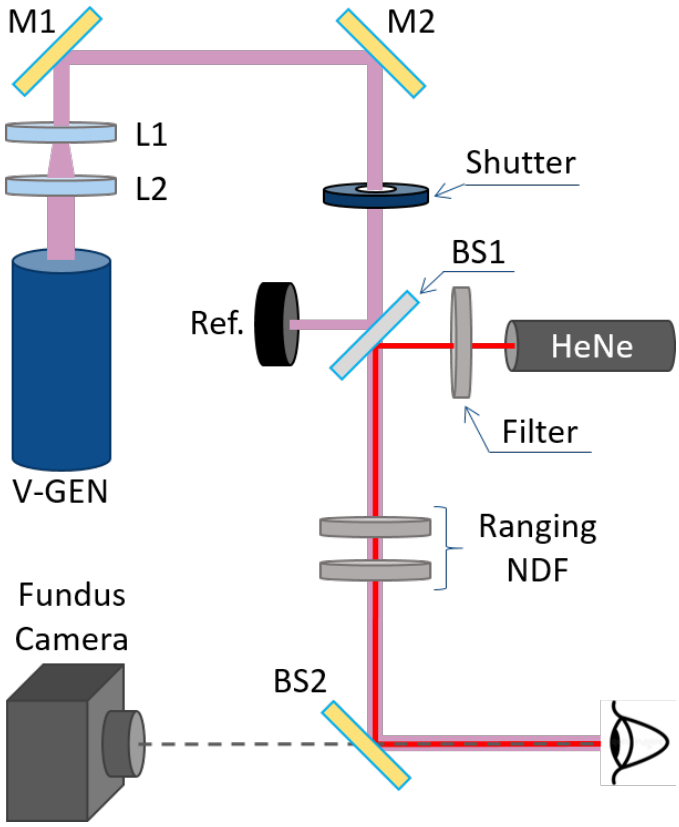

Figure 1. Exposure setup. L1: -20 mm focal length lens. L2: 50 mm focal length lens. NDF, Filter: neutral density filters. M1, M2: Nd:YAG laser line mirrors.

2.2.2 Beam Properties

Representative samples of the beam profile incident to the subject's cornea are shown in **Figure 2**. The beam diameter at the $1/e^2$ point was measured to be 2.5 ± 0.1 mm. The beam was well-collimated. Details of the measurement of the beam characteristics are in **APPENDIX B**.

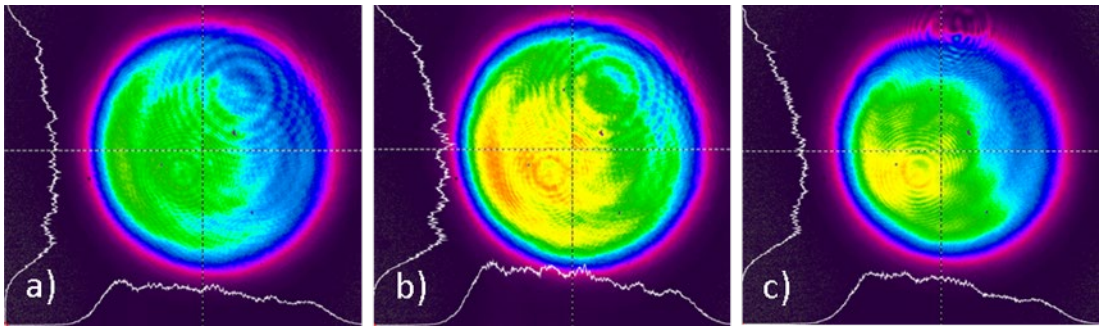

Figure 2. Representative beam profiles taken at a) 20%, b) 35%, and c) 85% of total available laser power at the pupil plane.

2.2.3 Estimate of Retinal Spot Size

The retinal beam spot size is estimated based on the schematic pig eye model of Coile and O'Keefe [6]. This model has a whole eye optical power of 78.2 D, with a refractive state of -1.5 D (myopic). A reduced-eye model therefore consists of a thin lens with an effective focal length of f_e = 1000/78.2 = 12.8 mm. Because of the slight myopia, the retinal plane is at a distance of 1000/(78.2 – 1.5) = 13 mm behind the lens, and approximately 0.2 mm behind the focal point of the lens.

Chromatic aberration adjusts the effective focal length due to dispersion in the refractive index of the lens. In a study of thermal lensing effects, Vincelette, et al. [7] examined the refractive error due to dispersion in near-infrared wavelengths. Their work indicates a refractive error R ~ 1.2 D at wavelengths near 1070 nm (referenced to R = 0 at 589 nm). Assuming the pig eye has the same refractive error, the optical power of the reduced-eye model is 78.2 – 1.2 = 77 D at 1070 nm, for an effective focal length of 1000/77 ~ 13 mm. Note that in this model, the dispersion in the NIR nearly cancels the myopia, and the 1070 nm light is essentially brought to focus at the retinal plane.

The beam in this experiment was well-collimated incident to the cornea. A diffraction-limited beam spot would therefore have a diameter at the retina given by $d_{ret} = 2.44\ \lambda\ f_e / D$, where λ is the wavelength, f_e is the effective focal length of the eye, and D is the beam diameter at the cornea. With λ = 1070 nm, f_e = 13 mm, and D = 2.5 mm, the diffraction-limited retinal beam spot has a diameter of approximately 14 μm. However, as noted in Section 3.2, the data do not support a retinal beam spot this small but indicate a retinal diameter several times larger.

2.2.4 Laser Exposure Procedure

2.2.4.1 Energy Calibration

Energy calibration was conducted on each day of scheduled exposures. Values were recorded for reference detector energy, energy at the target, and % laser setting at laser power setting increments ranging from 0 to 100% in steps of 5%. Plotting target energy against both reference energy and laser % determined the slope and y-intercept of a best linear fit for each. The respective coefficients calculated the approximate laser setting needed to produce a requested target energy prior to an exposure, and then to verify the energy delivered to the eye based on the recorded reference meter value for that exposure. The same calibration procedure was repeated after all exposures were completed, and the average of the two calibrations was the final reported energy for each exposure.

Uncertainties in the reported exposure dose were estimated by using the root-mean-square (RMS) of the relative residuals from the calibration data. That is,

$$\frac{\sigma_E}{E} \cong \sqrt{\frac{1}{N}\sum_{i=1}^{N}\left(\frac{r_i}{E_i}\right)^2}$$

where $r_i = (E_{fit} - E_{measured})$. Using this procedure across all calibration data produced a value of $\sigma_E/E = 0.0279$. In this report we round this up and report a relative error in energy measurements of 3%.

2.2.4.2 Selection of Exposure Sites

Retinal exposures were placed in the region within nominally 30° of the optic disk. A live video feed of the fundus, as seen through the fundus camera, selected exposure sites using retinal blood vessels as landmarks. The exposures were placed in areas free of retinal blood vessels (see **Figure 3**). Each eye had up to twenty-five exposures.

Prior to placing the animal in the exposure system, a Heidelberg SPECTRALIS (version 5.4.1) imaging platform collected images of the retina. The IR SLO channel of the SPECTRALIS collected a panoramic image of the retina. This image assisted in selecting and documenting exposure sites. During exposure procedures, each location was marked by hand on a printed panoramic image to help locate the exposure sites for post-exposure evaluation. **Figure 3** shows a representative sample of a baseline panoramic image of the retina marked with the location of exposure sites.

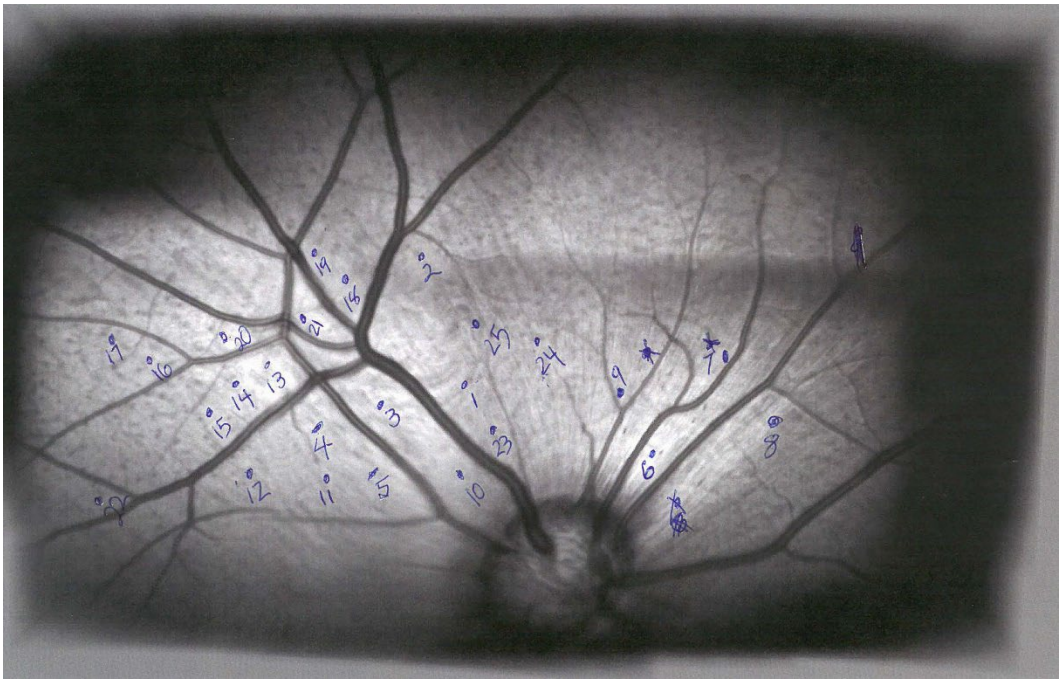

Figure 3. Example SLO panoramic view of a retina, marked with exposure sites.

2.2.5 Evaluation of Exposure Sites

One eye from each of the three subjects was specifically designated to determine the ED_{50} for inducing a minimal visible lesion (MVL). An MVL is defined to be any alteration of the retina detectable when viewing the retina through a fundus camera. These eyes were examined at nominally 1-hour and 24-hours post-exposure. At each of these two time points, three experienced

observers examined the exposure sites. Each observer was blind to the evaluation results of the other two observers. At least two of the three observers had to agree on the presence of a lesion to call a positive response for a particular exposure site. **Figure 4** shows examples of the non-hemorrhagic lesions at 1-hour and 24-hours post-exposure.

Studying the response to suprathreshold exposures used the second eye from each of the three subjects. Since the suprathreshold lesions appeared promptly, examinations were done only at 1-hour post-exposure, after which the subjects were euthanized. While the intent of the experiment was to measure the ED_{50} for creating contained retinal hemorrhages (CHL) and vitreal retinal hemorrhages (VHL), we did not observe any blood around the lesion sites that demonstrated a systematic dependence on the exposure dose. This finding is contrary to our earlier study using 1064 nm q-switched exposures [1]. It was therefore not possible to determine an ED_{50} for the hemorrhagic lesions. We observed no vitreal hemorrhage. We hypothesize that the CW beam essentially cauterized any damaged blood vessels. **Figure 5** shows examples of lesions caused by suprathreshold exposures 1-hour post-exposure.

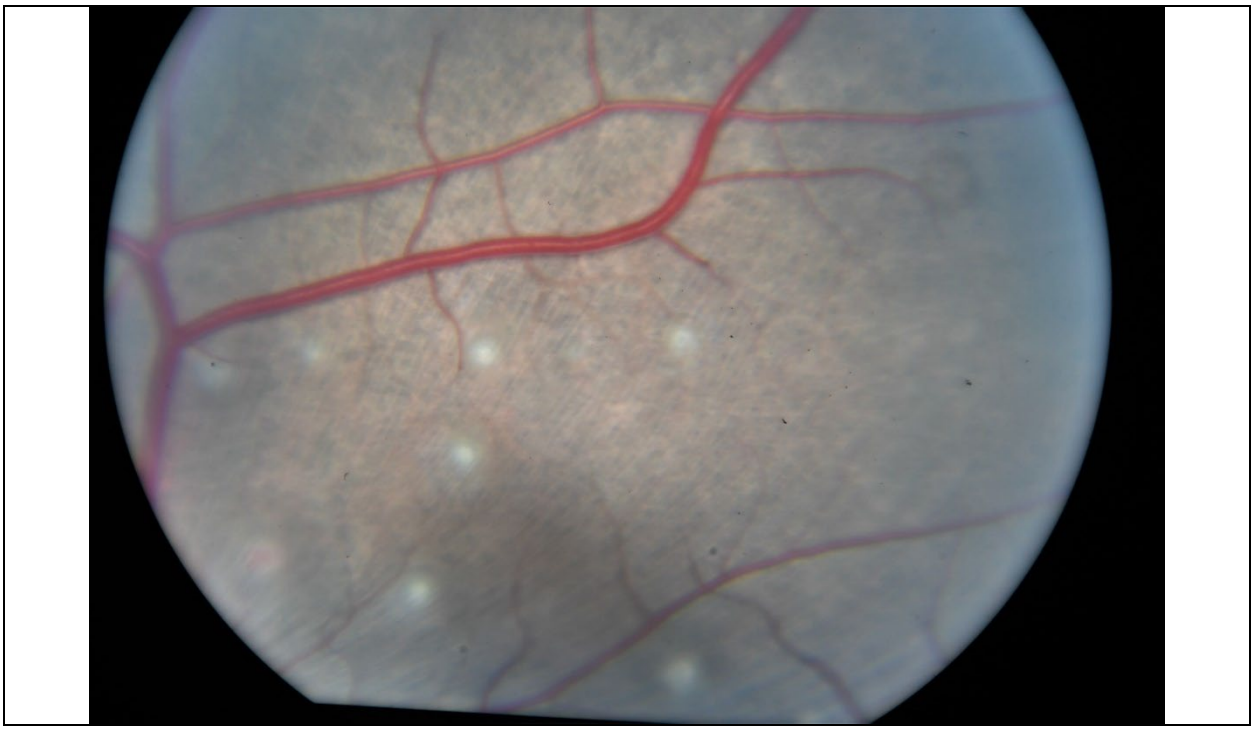

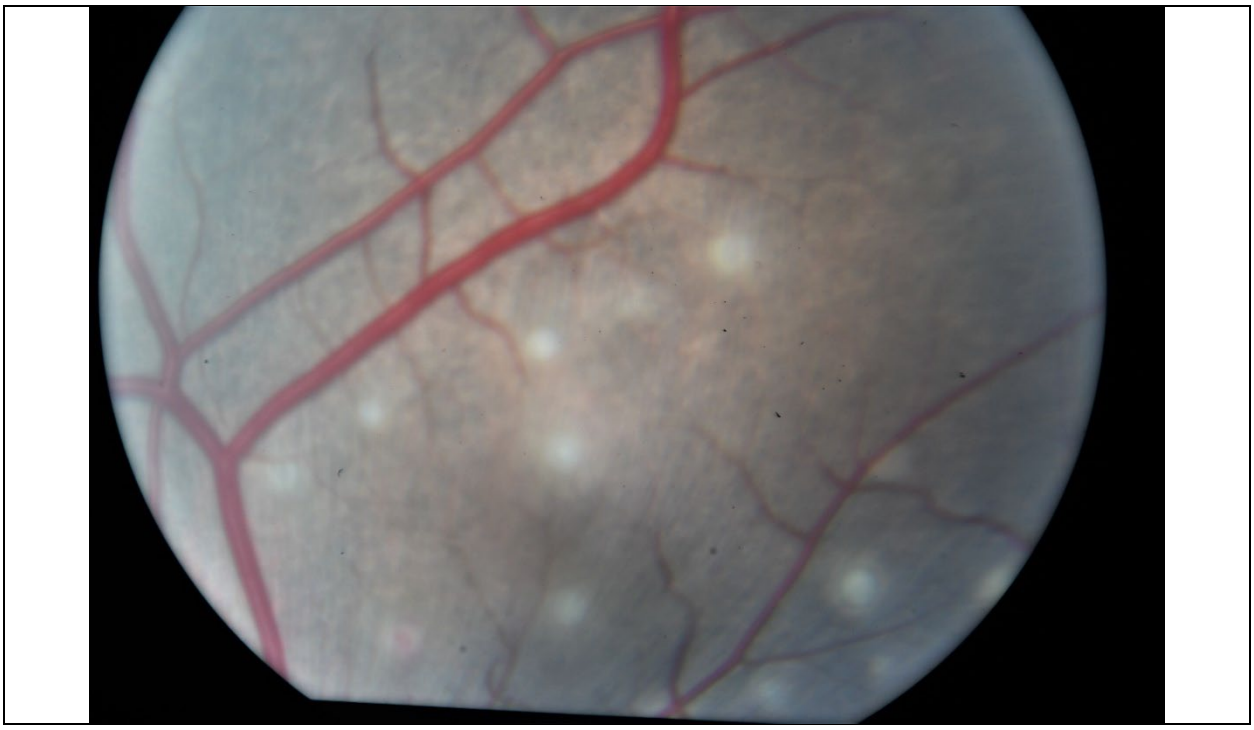

Figure 4. Example of lesions from near-threshold exposures to determine the MVL ED_{50}. Top: 1-hour post-exposure. Bottom: 24-hours post-exposure in the same eye.

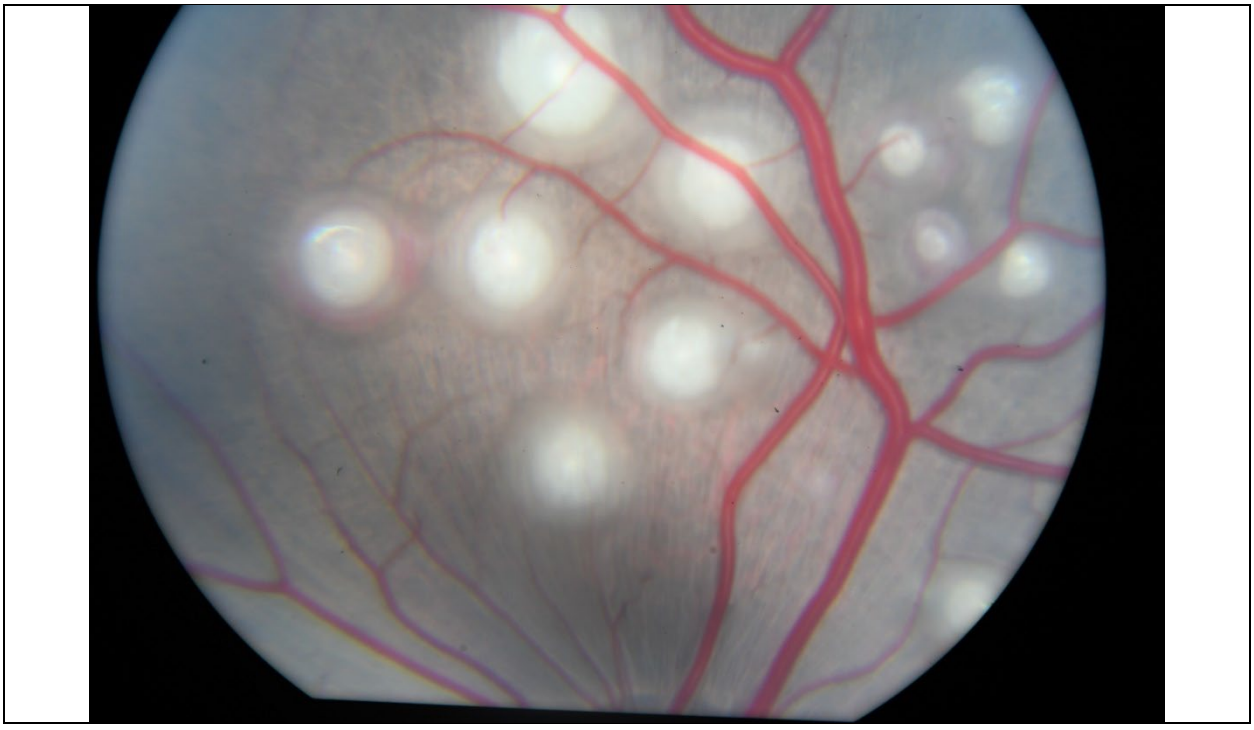

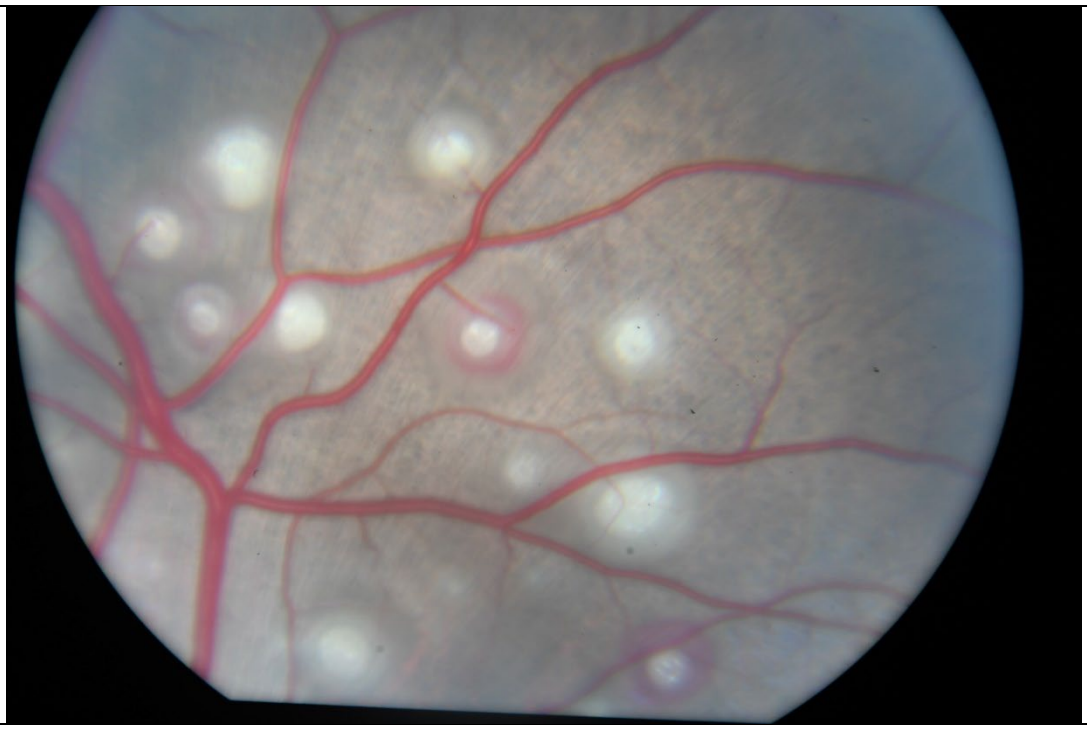

Figure 5. Lesions induced by suprathreshold exposures. Both images from the same eye (S21-003F OS).

2.3 Data Analysis

2.3.1 ED_{50} for Minimal Visible Lesion (MVL)

Data from the three eyes designated for determining the MVL ED_{50} were assembled into dose-response data sets for both the 1-hour and 24-hour post-exposure observations. These dose-response data sets are listed in **APPENDIX C**. Probit analysis [8] extracted the ED_{50} from this dose-response data set. The probit analysis also provided 95% confidence limits (fiducial limits) on the ED_{50}.

2.3.2 Lesion size for Suprathreshold Exposures

No vitreal hemorrhages (VHL) were observed. A few lesions with reddening around them were observed, indicating contained hemorrhages (CHL). However, the doses at which this appeared showed no repeatability that would enable determination of a threshold. Rather, the retinal location exposed seemed to be the significant factor. Our hypothesis is that the higher power CW beam cauterized impacted retinal vasculature, suppressing any hemorrhage.

The lesion size, as observed in fundus photographs, exhibited a robust dependence on the energy dose of the exposure. Measurement of the lesion size (extent) explored this, as described in **APPENDIX D**.

3 RESULTS AND DISCUSSION

3.1 ED_{50} for Minimal Visible Lesion

The ED_{50} for inducing an MVL from a 100 ms exposure to a 1070 nm CW laser beam is listed in **Table 1**. The ED_{50} is reported for 1-hour and 24-hour post-exposure evaluation of the retina, consistent with modern practice. Details of the probit analysis are in **APPENDIX C**.

Table 1. ED_{50} for inducing a MVL from a 100 ms exposure to a 1070 nm CW laser.

End point	# Exposures (positive, negative responses)	ED_{50} (mJ TIE*)	Fiducial Limits (mJ TIE)	Probit Slope
1-hour post-exposure	75 (42, 33)	26.2	[18.0 – 34.5]	2.64
24-hour post exposure	75 (39, 36)	29.9	[23.8 – 36.7]	3.89

*Total Intraocular Energy

There are few comparable MVL ED_{50} measurements made in Non-Human Primate (NHP) eyes with which to compare our results. A few of these are listed in **Table 2**. The most directly comparable measurement is that from Skeene et al. [9] with our ED_{50} based on the 1-hour post-exposure observations, where the ratio of the pig ED_{50} to the NHP ED_{50} is 3.9.

Table 2. MVL ED_{50} measured in Rhesus macaques for CW exposures near 100 ms and 1070 nm.

λ (nm)	*t* (ms)	ED_{50} (mJ)	Criterion	Notes	Source
1060	100	6.7 ± 0.3	1 hour	minimal spot?	Skeene et al. [9]
1060	150	16.5 ± 1.5	immediate	30 μm retinal spot diameter	Birngruber et al. [10]

In our previous report [1], we compared the ED_{50} in the pig and the paramacular region of the NHP eye for q-switched exposures to 1064 nm pulses. Some of this data is reproduced in **Table 3**. The ratio of the ED_{50} in the pig to the NHP is 3.9, consistent for both q-switched and CW exposures at the 1-hour post-exposure endpoint at a 1064 nm wavelength.

Table 3. Comparison of the ED_{50} for q-switched exposures to 1064 nm pulses in the pig and paramacular macaque retinas.

End point	ED_{50} – Yucatan Min-Pig*	ED_{50} – Rhesus macaque**	ED_{50} Ratio pig/macaque
1 hour	214 μJ	55.4 μJ	3.9
24 hours	193 μJ	44.6 μJ	4.3

*7 ns, 1064 nm (Schmidt et al [1]).
**16 ns, 1064, paramacular (Greiss et al. [11])

3.2 Suprathreshold lesion size dependence on dose

The extent of the lesions caused by suprathreshold exposures demonstrates a direct correlation to the incident dose. **Figure 6** shows a plot of the geometric mean of the lesion diameter as a function of the total intraocular energy (TIE), i.e., the energy of the 100 ms pulse incident to the cornea. The data for this figure are in **APPENDIX D**. Note that the suprathreshold doses were as great as 1 J TIE, over 30 times the MVL ED_{50}.

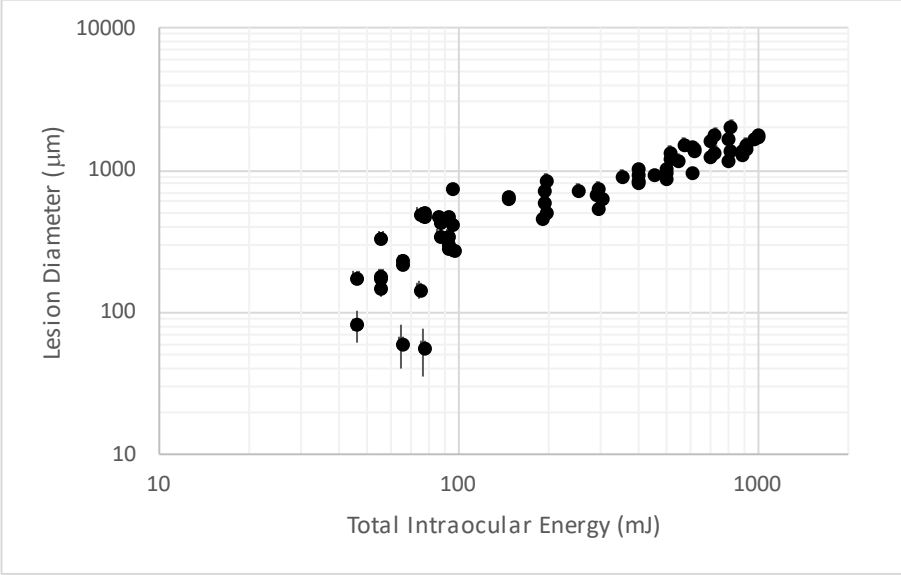

Figure 6. Lesion size vs. Dose for suprathreshold exposures to a 1070 nm CW laser.

The beam incident to the cornea was well-collimated, with a $1/e^2$ diameter of 2.5 mm. The diffraction-limited beam diameter at the retina, assuming a 13 mm effective focal length [6], is about 14 μm. The MVL ED_{50} was found to be about 30 mJ. A rough extraction of the downward curve toward the lower-energy end of the lesion size curve of **Figure 6** suggests a minimum spot size on the order of 4 or 5 times this value (55 μm to 70 μm) may be more realistic. In a review of the retinal spot-size dependence of retinal injury thresholds, Lund et al. [12] noted that, for a wide range of exposure durations, the ED_{50} is nearly constant for retinal irradiance diameter less than about 100 μm. They theorized this may be due to ocular aberrations and intraocular scattering of light before reaching the retina. However, it does suggest, as does our 1070 nm, 100 ms data, that the minimum retinal beam size is significantly larger than a diffraction-limited spot. This becomes important for modeling considerations.

4 SUMMARY AND CONCLUSIONS

Threshold and suprathreshold retinal effects from exposure to 100 ms pulses from a continuous-wave Nd:YAG laser (λ = 1070 nm) were investigated in a Yucatan mini-pig model. The measured

ED_{50} for inducing a minimal visible lesion (MVL) for exposure to a collimated beam was 29.9 mJ total intraocular energy (TIE). This value is approximately four times higher than a similar measurement in a Rhesus macaque retina. A similar ratio was observed for 1064 nm q-switched pulses [1].

Thresholds for hemorrhagic effects could not be determined, even for doses as large as 1 J TIE (over 30 times the MVL ED_{50}). A plausible hypothesis is the CW beam cauterizes damaged blood vessels, preventing leakage of blood into the retina or vitreous. However, a correlation exists between the size, or extent, of the retinal lesion with the pulse energy. This data can serve as an important check on extending computational models to include suprathreshold effects.

This study highlights the importance of identifying retinal hazards associated with Nd:YAG laser sources and provides guidance for future experimentation to identify the extent of the damage. A histological study could be performed to assess the layers of the retina and the corresponding cellular effects. Additionally, a modeling study could be performed to provide a basis for dose-correlated prediction of injury. Together with the results of these experiments, these tools can further inform the standards for safe use of lasers, inform postexposure treatment plans, and provide a vast dataset for refinement and validation of efforts to computationally model laser bioeffects.

5 REFERENCES

[1] Morgan S. Schmidt, Benjamin A. Rockwell, Aurora D. Shingledecker, Brian J. Lund, Gary D. Noojin, Kurt J. Schuster, Heuy-Ching Wang, Peter R. Edsall, W. Rowe Elliot and Amanda J. Tijera, Suprathreshold Retinal Lesions Induced by a Q-switched Nd:YAG Laser in a Yucatan Mini-Pig Model: Contained vs. Vitreal Hemorrhage, (2020) Air Force Research Laboratory Technical Report AFRL-RH-FS-TS-2020-0008.

[2] Department of Defense (DoD). (2010). *Use of Animals in DoD Programs* (DoD Instruction Number 3216.01). Retrieved February 21, 2017, from http://www.dtic.mil/whs/directives/corres/pdf/321601p.pdf

[3] USDA Animal Welfare Regulations, 9 C.F.R. Subchapter A (2013). Retrieved February 21, 2017, from https://www.nal.usda.gov/awic/animal-welfare-act

[4] National Research Council (NRC). (2011). *Guide for the Care and Use of Laboratory Animals* (8th ed.). Washington, DC: National Academies Press.

[5] The Care and Use of Laboratory Animals in DOD Programs, AFMAN 40-401(1) (2005). Retrieved February 21, 2017, from http://www.apd.army.mil/pdffiles/r40_33.pdf

[6] D.C. Coile and L.P. O'Keefe, "Schematic eyes for domestic animals", Ophthal. Physiol. Opt., 8:215:220 (1988).

[7] R.L. Vincelette, A.J. Welch, R.J. Thomas, B.A. Rockwell and D.J. Lund, "Thermal lensing in ocular media exposed to continuous-wave near-infrared radiation: the 1150-1350-nm range", *J. Biomed. Opt.* 13(5):054005 (2008).

[8] D.J. Finney, *Probit Analysis*, Cambridge University Press, New York (1971).

[9] C.H. Skeene, W.R. Bruce, H.H. Tips, M.G. Smith and G.G. Garza, Ocular Effects of Near Infrared Laser Radiation for Safety Criteria. Technology Incorporated, Contract F41609-71-C-0016. USAF School of Aerospace Medicine, Final Report, June 1972.

[10] R. Birngruber, V.-P. Gabel and F. Hillenkamp, "Experimental studies of laser thermal retinal injury," *Health Phys*. 44(5):519:531 (1983).

[11] G.A. Greiss, M.F. Blankenstein and G.G. Williford, "Ocular Damage from Multiple-Pulse Laser Exposures," *Health Phys.* 39:921-927 (1980).

[12] D.J. Lund, P. Edsall, B.E. Stuck and K. Schulmeister, "Variation of laser-induced retinal thresholds with retinal irradiated area: 0.1-s duration, 514-nm exposures," *J. Biomed. Opt.* 12(2):024023 (2007).

[13] C.P. Cain, L. Manning and G.D. Noojin, "A comparison of various probit methods for analyzing yes/no data on a log scale," AL/OE-TR-1996-0102:46 (1996).

APPENDIX A List of Detectors and Energy Meters

The detectors and meters used to perform calibration and dosimetry for the retinal laser exposures are listed in **Table 4**. All detectors were NIST-calibrated at the time of their use. The Reference detector (labeled 'Ref' in **Figure 1**) was a permanent part of the setup. The Target detector was placed in the eye position each exposure day prior to placing an animal subject in the exposure setup to calibrate the Reference detector.

Table 4. Detectors and energy meters used for beam dosimetry

Purpose	Manufacturer	Model
Target detector (MVL)	Coherent	PM3
Target detector (Supra)	Coherent	PM10
Target meter	Coherent	LabMax
Reference detector	Coherent	PM3
Reference meter	Coherent	LabMax

APPENDIX B Beam Profile Measurements

This appendix details the methods and equipment used to measure the characteristics of the beam incident to the cornea of the test subject.

Equipment Used

Table 5 lists the equipment used to measure the beam characteristics. All equipment was NIST-calibrated at the time of use.

Table 4. Equipment used to characterize the Spectra Physics VGEN-C-20 Laser

Item	Manufacturer
Neutral Density Filters (absorptive)	ThorLabs
TDX220 Oscilloscope	Tektronix
DET10D Photodiode	Thorlabs
SP 620U Profiling Camera	Spiricon Inc.

Pulse Width Measurement

A ThorLabs DET10D indium gallium arsenide (InGaAs) photodiode sensitive to 1 um light in conjunction with a Tektronix TDX220 oscilloscope identified the leading and trailing edges of several individual pulses from the VGEN-C-20 laser. The timestamp of each leading and trailing edge was identified using the cursor on the oscilloscope and recorded. The differences between the recorded leading and trailing edge for each pulse were all equal 100 ms.

Beam Diameter Measurement

The collimated beam diameter was measured and verified before and after all experimental data was collected. Beam measurements were made using the Spiricon Profiling Camera listed in **Table 5** in conjunction with Spiricon beam analysis software. The software used the D4σ method to determine the horizontal and vertical extent of the beam. The beam profile was measured from underneath the final beam splitter. This allowed measurement at the approximate pupil plane distance instead of further down the beam path. Representative beam profiles are shown in **Figure 7**.

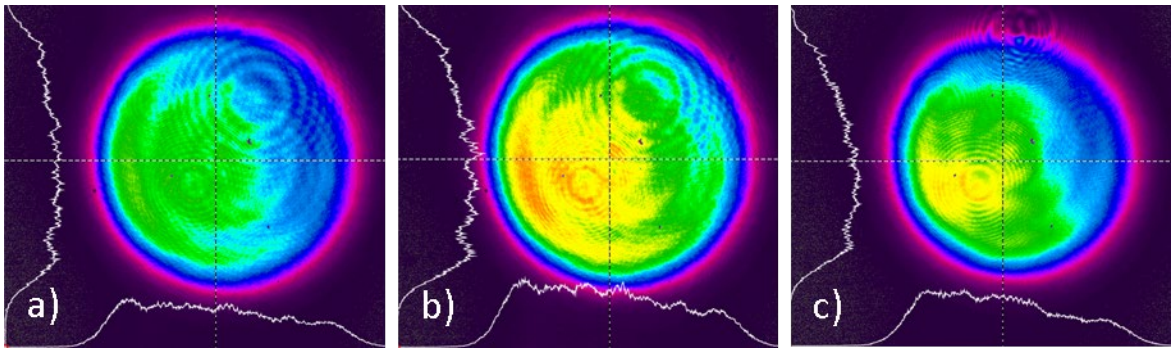

Figure 7. CW beam profile near the pupil plane of the fundus camera for a) 20%, b) 35%, and c) 85% of maximum laser power.

The average beam diameter at each laser power setting is the geometric mean of the average x- and y-dimension diameters over three frames. The resulting beam diameters are listed in Table 6. The standard deviation of these measurements, 0.07, is used as a measure of the uncertainty in the beam diameter. Here we round up to the nearest 0.1 cm when reporting the beam size. Based on these measurements, we report a beam diameter of 2.5 ± 0.1 mm.

Table 5. Summary of the results of the beam diameter measurements at the fundus camera pupil plane.

% Max laser power	Avg. Width X	Avg. Width Y	Diameter (mm)
10%	2.61	2.61	2.61
20%	2.63	2.64	2.63
35%	2.56	2.55	2.56
55%	2.48	2.45	2.46
85%	2.47	2.46	2.46
100%	2.52	2.53	2.52
Average:	2.55	2.54	2.54
St. Dev.	0.06	0.07	0.07

APPENDIX C Dose-Response Data and Probit Analysis for MVL Data

This appendix contains the raw dose-response data used to determine the ED_{50} for causing a minimal visible lesion, based on the 1-hour and 24-hour post-exposure evaluations. Also included are details of the results of a probit analysis on each of the data sets. Probit version 2.1.3 [13] performed the probit analysis. Plots of the raw data with the probit dose-response curves superimposed are included. The graphs also show the 95% confidence limits on the fitted dose-response curves.

C.1 Minimal Visible Lesion – 1-hour post-exposure evaluation

C.1.1 Dose-response data

Table 6. Dose-response data for Minimal Visible Lesion. 1-hour post-exposure evaluation. All energies ±3%.

Energy (mJ)	Lesion	Subject	Energy (mJ)	Lesion	Subject	Energy (mJ)	Lesion	Subject
9.56	0	S21-002F_OD	24.87	0	S21-003F_OD	45.76	1	S21-003F_OD
9.56	0	S21-002F_OD	24.87	1	S21-003F_OD	45.76	0	S21-003F_OD
9.56	0	S21-002F_OD	24.87	1	S21-003F_OD	45.76	1	S21-003F_OD
9.56	0	S21-002F_OD	28.17	0	S21-001F_OD	45.76	1	S21-003F_OD
9.61	0	S21-001F_OD	28.17	0	S21-001F_OD	45.76	1	S21-003F_OD
9.61	1	S21-001F_OD	28.17	0	S21-001F_OD	48.32	1	S21-001F_OD
13.99	0	S21-001F_OD	28.17	0	S21-001F_OD	48.32	1	S21-001F_OD
13.99	0	S21-001F_OD	29.64	0	S21-002F_OD	50.39	0	S21-002F_OD
14.65	1	S21-003F_OD	29.64	1	S21-002F_OD	50.39	1	S21-002F_OD
14.65	0	S21-003F_OD	29.64	1	S21-002F_OD	50.39	1	S21-002F_OD
14.65	1	S21-003F_OD	29.64	0	S21-002F_OD	56.32	1	S21-003F_OD
14.65	0	S21-003F_OD	29.64	1	S21-002F_OD	56.32	1	S21-003F_OD
18.45	0	S21-001F_OD	33.42	0	S21-001F_OD	56.32	1	S21-003F_OD
18.45	1	S21-001F_OD	35.26	1	S21-003F_OD	56.32	1	S21-003F_OD
18.45	0	S21-001F_OD	35.26	1	S21-003F_OD	58.61	1	S21-001F_OD
18.45	0	S21-001F_OD	35.26	0	S21-003F_OD	58.61	0	S21-001F_OD
18.45	0	S21-001F_OD	35.26	1	S21-003F_OD	58.61	1	S21-001F_OD
19.48	0	S21-002F_OD	38.15	1	S21-001F_OD	60.85	0	S21-002F_OD
19.48	0	S21-002F_OD	38.15	1	S21-001F_OD	60.85	1	S21-002F_OD
19.48	0	S21-002F_OD	38.15	0	S21-001F_OD	60.85	1	S21-002F_OD
19.48	1	S21-002F_OD	39.97	0	S21-002F_OD	66.89	1	S21-003F_OD
19.48	1	S21-002F_OD	39.97	1	S21-002F_OD	66.89	1	S21-003F_OD
23.56	1	S21-001F_OD	39.97	0	S21-002F_OD	66.89	1	S21-003F_OD
23.56	0	S21-001F_OD	39.97	1	S21-002F_OD	66.89	1	S21-003F_OD
24.87	1	S21-003F_OD	39.97	1	S21-002F_OD	69.56	1	S21-001F_OD

C.1.2 Probit analysis

Table 7. Probit analysis of 1-hour post-exposure MVL data.

RHDO-20-07, 1070 nm, 100 ms, 1-hour observation

Threshold
ED50: 26.3 [18.0 – 34.5]

Fit Results
Slope 2.64
Intercept -3.75
Chi-squared: 17.1042 on 21 degrees of freedom (P = 0.6462)

Diagnostics
H: 1.00 g: 0.26 t: 1.96
Log xbar: 1.48 log ybar: 5.16
S0: 40.908 Sxx: 2.104 Sxy: 5.560 Syy: 31.794

Probability Curve

Prob	ED[P] Dose	Lower Limit	Upper Limit	Prob	ED[P] Dose	Lower Limit	Upper Limit
0.01	3.45	0.345	7.41	0.55	29.2	21.2	39.4
0.02	4.37	0.559	8.71	0.6	32.6	24.5	46
0.03	5.08	0.759	9.65	0.65	36.6	28	55.1
0.04	5.69	0.955	10.4	0.7	41.3	31.6	67.6
0.05	6.24	1.15	11.1	0.75	47.1	35.6	85.6
0.06	6.75	1.35	11.7	0.8	54.5	40.2	113
0.07	7.23	1.55	12.3	0.85	64.6	45.9	156
0.08	7.69	1.75	12.8	0.9	80	53.7	238
0.09	8.14	1.96	13.3	0.91	84.2	55.7	263
0.1	8.57	2.18	13.8	0.92	89.1	58	295
0.15	10.6	3.34	16.1	0.93	94.7	60.6	333
0.2	12.6	4.67	18.2	0.94	101	63.7	382
0.25	14.5	6.21	20.3	0.95	110	67.3	448
0.3	16.6	7.99	22.5	0.96	120	71.7	539
0.35	18.7	10	24.9	0.97	135	77.6	677
0.4	21	12.4	27.5	0.98	157	86.1	918
0.45	23.5	15	30.6	0.99	199	101	1.49E+03
0.5	26.2	18	34.5				

C.2 Minimal Visible Lesion – 24-hour post-exposure evaluation

C.2.1 Dose-response data

Table 8. Dose-response data for Minimal Visible Lesion, 24-hour post-exposure evaluation. All energies ± 3%.

Energy (mJ)	Lesion	Subject	Energy (mJ)	Lesion	Subject	Energy (mJ)	Lesion	Subject
9.56	0	S21-002F_OD	24.87	0	S21-003F_OD	45.76	1	S21-003F_OD
9.56	0	S21-002F_OD	24.87	1	S21-003F_OD	45.76	0	S21-003F_OD
9.56	0	S21-002F_OD	24.87	1	S21-003F_OD	45.76	1	S21-003F_OD
9.56	0	S21-002F_OD	28.17	0	S21-001F_OD	45.76	1	S21-003F_OD
9.61	0	S21-001F_OD	28.17	1	S21-001F_OD	45.76	1	S21-003F_OD
9.61	0	S21-001F_OD	28.17	0	S21-001F_OD	48.32	1	S21-001F_OD
13.99	0	S21-001F_OD	28.17	0	S21-001F_OD	48.32	1	S21-001F_OD
13.99	0	S21-001F_OD	29.64	0	S21-002F_OD	50.39	0	S21-002F_OD
14.65	1	S21-003F_OD	29.64	1	S21-002F_OD	50.39	1	S21-002F_OD
14.65	0	S21-003F_OD	29.64	0	S21-002F_OD	50.39	1	S21-002F_OD
14.65	1	S21-003F_OD	29.64	0	S21-002F_OD	56.32	1	S21-003F_OD
14.65	0	S21-003F_OD	29.64	1	S21-002F_OD	56.32	1	S21-003F_OD
18.45	0	S21-001F_OD	33.42	0	S21-001F_OD	56.32	1	S21-003F_OD
18.45	0	S21-001F_OD	35.26	1	S21-003F_OD	56.32	1	S21-003F_OD
18.45	0	S21-001F_OD	35.26	1	S21-003F_OD	58.61	1	S21-001F_OD
18.45	0	S21-001F_OD	35.26	0	S21-003F_OD	58.61	0	S21-001F_OD
18.45	0	S21-001F_OD	35.26	1	S21-003F_OD	58.61	0	S21-001F_OD
19.48	0	S21-002F_OD	38.15	1	S21-001F_OD	60.85	1	S21-002F_OD
19.48	0	S21-002F_OD	38.15	1	S21-001F_OD	60.85	1	S21-002F_OD
19.48	0	S21-002F_OD	38.15	1	S21-001F_OD	60.85	1	S21-002F_OD
19.48	0	S21-002F_OD	39.97	0	S21-002F_OD	66.89	1	S21-003F_OD
19.48	0	S21-002F_OD	39.97	1	S21-002F_OD	66.89	1	S21-003F_OD
23.56	1	S21-001F_OD	39.97	0	S21-002F_OD	66.89	1	S21-003F_OD
23.56	0	S21-001F_OD	39.97	1	S21-002F_OD	66.89	1	S21-003F_OD
24.87	1	S21-003F_OD	39.97	1	S21-002F_OD	69.56	1	S21-001F_OD

C.2.2 Probit analysis

Table 9. Probit analysis of 24-hour post-exposure MVL data

RHDO-20-07, 1070 nm, 100 ms, 24-hour observation

Threshold
ED50: 29.9 [23.8 – 36.7]

Fit Results
Slope 3.89
Intercept -5.74
Chi-squared: 26.2854 on 21 degrees of freedom (P = 0.1566)

Diagnostics
H: 1.00 g: 0.17 t: 1.96
Log xbar: 1.50 log ybar: 5.10
S0: 35.934 Sxx: 1.453 Sxy: 5.649 Syy: 48.251

Probability Curve

Prob	ED[P] Dose	Lower Limit	Upper Limit	Prob	ED[P] Dose	Lower Limit	Upper Limit
0.01	7.55	2.61	11.9	0.55	32.3	26.1	40.1
0.02	8.87	3.43	13.4	0.6	34.8	28.5	44.1
0.03	9.83	4.08	14.4	0.65	37.6	31	49.1
0.04	10.6	4.64	15.3	0.7	40.9	33.6	55.2
0.05	11.3	5.16	16	0.75	44.6	36.5	63.1
0.06	11.9	5.64	16.6	0.8	49.3	39.8	73.6
0.07	12.5	6.1	17.2	0.85	55.3	43.7	88.5
0.08	13	6.54	17.8	0.9	64	49.1	112
0.09	13.5	6.97	18.3	0.91	66.2	50.4	119
0.1	14	7.39	18.8	0.92	68.8	51.9	127
0.15	16.2	9.4	21	0.93	71.8	53.6	136
0.2	18.2	11.3	23	0.94	75.2	55.5	147
0.25	20.1	13.3	25	0.95	79.3	57.8	160
0.3	22	15.3	27	0.96	84.4	60.6	178
0.35	23.8	17.3	29	0.97	91.2	64.2	203
0.4	25.8	19.4	31.3	0.98	101	69.2	241
0.45	27.8	21.6	33.8	0.99	119	77.9	317
0.5	29.9	23.8	36.7				

C.3 Graphs of fits to MVL data

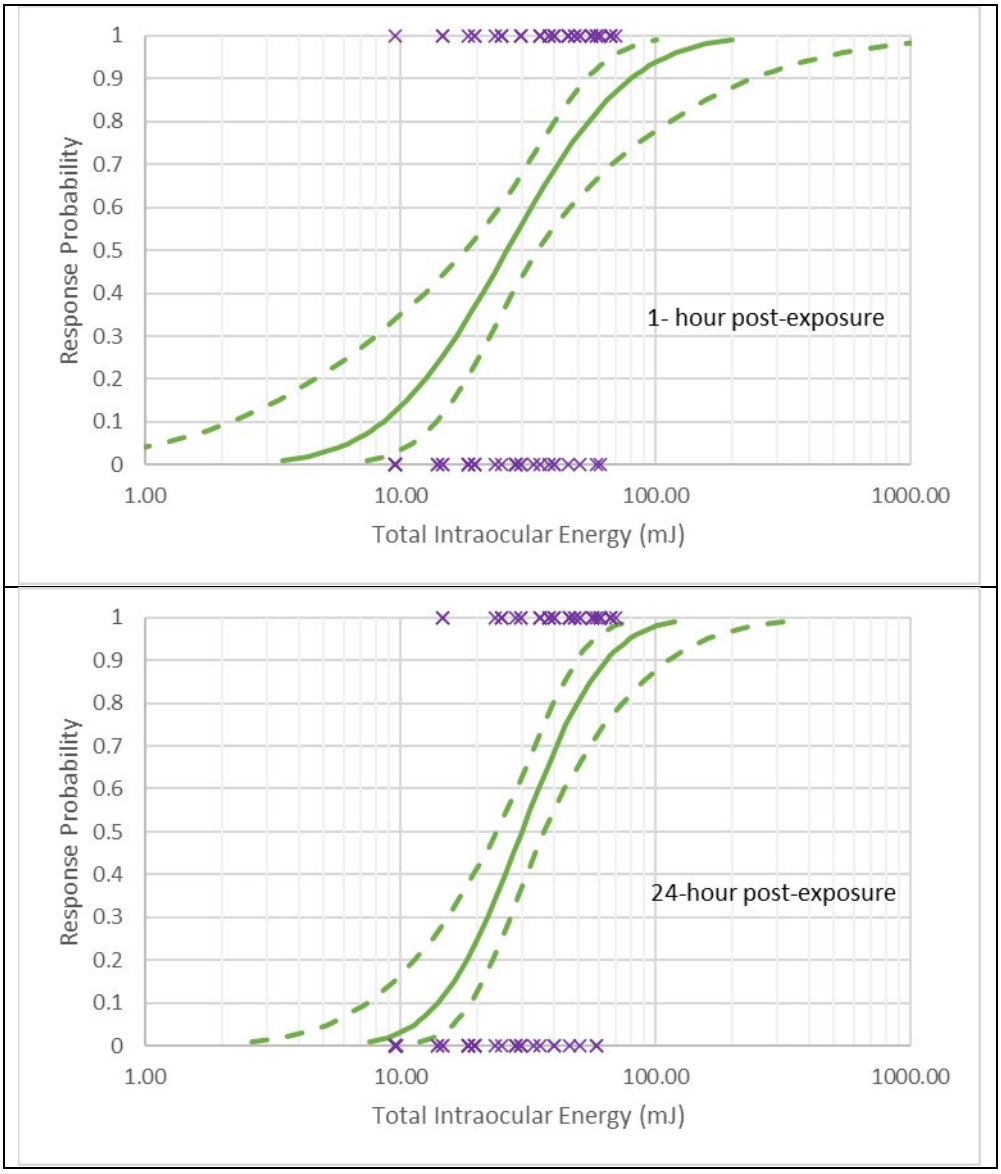

Figure 8. Probit fits to MVL data. Top: 1-hour post-exposure observation. Bottom: 24-hour post-exposure observation.

APPENDIX D Lesion Size for Suprathreshold Exposures

Lesion sizes were measured from the fundus photos of the three eyes receiving the suprathreshold exposures. These photos were captures with a 50° field of view. ImageJ software imported the fundus images, where the horizontal and vertical extent of the lesions were marked and measured in pixels. An example of the lesions marked for measurement is shown in **Figure 9**. The extent of the full 50° fundus image was 5210 pixels, used to convert the lesion measurements into degrees in the FOV. Converting the lesion sizes to units of length used the schematic pig eye model of Coile and O'Keefe [6]. In this model, the retinal image in the pig eye has a size of 0.2298 mm/deg. The final scale is 2.197 μm/pixel.

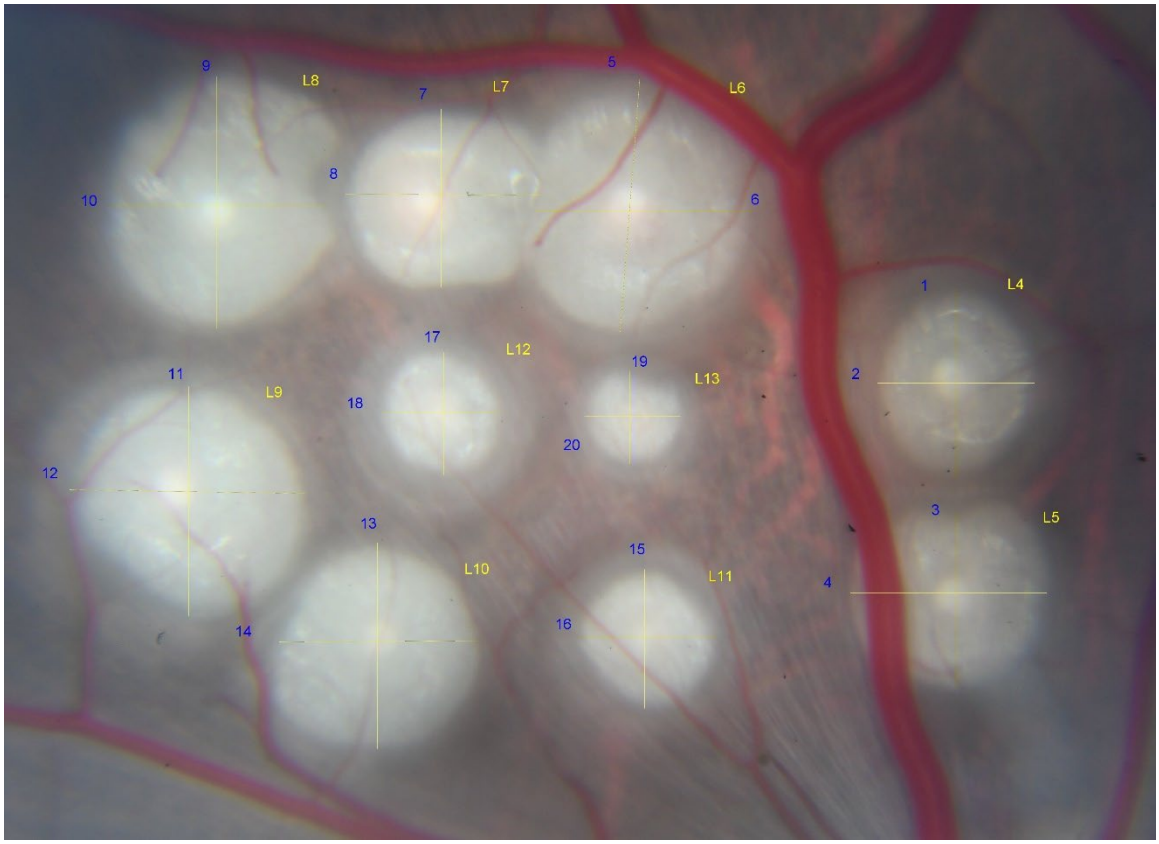

Figure 9. Lesions in the fundus of the left eye of S21-001F, marked for measurement of the lesion extent.

The horizontal and vertical extents of the suprathreshold lesions are listed in **Table 11** as a function of the Total Intraocular Energy of the exposure, along with the geometric mean of the horizontal and vertical extents. Uncertainties in these measurements were estimated by making repeated, independent measurements on a selection of lesions. These uncertainties therefore include the consistency in placing the lines used to make the measurements in ImageJ, as well as consistency in defining the margins of the lesions. An uncertainty in the horizontal and vertical lesion size measurements of ±30 μm was determined from this process.

Table 10. Lesion extent data. Subject is abbreviation for S21-XXXF_OS. All energies ± 3%. All vertical and horizontal measurements ± 30 μm.

TIE (mJ)	Lesion Extent			Subject	TIE (mJ)	Lesion Extent			Subject
	Horz. (μm)	Vert. (μm)	Geom. Mean (μm)			Horz. (μm)	Vert. (μm)	Geom. Mean (μm)	
495	881	852	866 ± 21	001F	999	1836	1705	1769 ± 21	002F
599	950	976	963 ± 21	001F	999	1863	1626	1740 ± 21	002F
696	1221	1309	1265 ± 21	001F	907	1683	1407	1539 ± 21	002F
794	1090	1274	1178 ± 21	001F	811	2007	2116	2061 ± 21	002F
883	1344	1459	1400 ± 21	001F	714	1195	1503	1340 ± 21	002F
967	1696	1636	1666 ± 21	001F	610	1415	1388	1401 ± 21	002F
883	1213	1365	1287 ± 21	001F	505	1213	1213	1213 ± 21	002F
794	1767	1598	1680 ± 21	001F	399	1072	975	1023 ± 21	002F
696	1652	1646	1649 ± 21	001F	293	814	693	751 ± 21	002F
599	1417	1503	1459 ± 21	001F	194	710	734	721 ± 21	002F
495	967	975	971 ± 21	001F	93	492	448	470 ± 21	002F
395	874	844	859 ± 21	001F	46	186	168	177 ± 21	003F
290	670	687	679 ± 21	001F	55	369	308	337 ± 21	003F
190	457	452	455 ± 21	001F	65	57	66	61 ± 21	003F
93	348	343	345 ± 21	001F	76	62	53	57 ± 21	003F
93	308	308	308 ± 21	001F	86	466	484	475 ± 21	003F
86	326	369	347 ± 21	001F	96	765	721	743 ± 21	003F
74	413	597	497 ± 22	001F	146	633	624	628 ± 21	003F
65	229	211	220 ± 21	001F	197	995	747	862 ± 22	003F
55	211	158	183 ± 22	001F	250	651	812	727 ± 21	003F
55	158	195	176 ± 21	001F	301	616	677	645 ± 21	003F
65	237	228	233 ± 21	001F	351	1002	836	915 ± 21	003F
74	162	132	146 ± 21	001F	399	861	800	830 ± 21	003F
86	422	450	435 ± 21	001F	449	977	896	936 ± 21	003F
96	264	282	273 ± 21	001F	146	677	633	655 ± 21	003F
93	292	274	283 ± 21	002F	96	431	404	417 ± 21	003F
194	599	580	589 ± 21	002F	76	501	510	505 ± 21	003F
293	520	582	551 ± 21	002F	494	1066	993	1029 ± 21	003F
399	1011	897	952 ± 21	002F	538	1241	1128	1183 ± 21	003F
505	1398	1309	1353 ± 21	002F	564	1626	1467	1545 ± 21	003F
610	1476	1337	1405 ± 21	002F	46	88	79	83 ± 21	003F
714	1974	1634	1796	002F	76	457	492	474 ± 21	003F
811	1450	1284	1364	002F	55	167	132	149 ± 22	003F
907	1318	1573	1440	002F	197	492	510	501 ± 21	003F